2D Encapsulation in Multiphase Polymers: Role of Viscoelastic, Geometrical and Interfacial Properties

ARTICLE *in* MACROMOLECULES · JANUARY 2012

Impact Factor: 5.8 · DOI: 10.1021/ma201151k

3 AUTHORS:

Khalid Lamnawar
Institut National des Sciences Appliquées de…
51 PUBLICATIONS **325** CITATIONS
SEE PROFILE

Mosto Bousmina
Euro-Mediterranean Université of Fez
217 PUBLICATIONS **5,343** CITATIONS
SEE PROFILE

Abderrahim Maazouz
Institut National des Sciences Appliquées de…
154 PUBLICATIONS **1,050** CITATIONS
SEE PROFILE

Macromolecules

ARTICLE

pubs.acs.org/Macromolecules

2D Encapsulation in Multiphase Polymers: Role of Viscoelastic, Geometrical and Interfacial Properties

Khalid Lamnawar,[†] Mosto Bousmina,[§] and Abderrahim Maazouz*[,‡,§]

[†]Laboratoire de Mécanique des Contacts et des Structures, Université de Lyon, CNRS, INSA-Lyon, LaMCoS UMR CNRS#5259, Groupe de Recherche Pluridisciplinaire en Plasturgie, F69621, France

[‡]Université de Lyon, F-69361 Lyon, and CNRS, UMR 5223, Ingénierie des Matériaux Polymères, INSA Lyon, F-69621 Villeurbanne, France

[§]Hassan II Academy of Science and Technology, Postal Code 10 100, Rabat, Morocco

ABSTRACT: The aim of the present work has been to gain a fundamental understanding of the mechanisms governing encapsulation in the multiphase systems as a blend or multilayer structures. The model systems chosen for this study are based on (i) Newtonian poly(dimethylsiloxane) polymers of varying molar masses and (ii) high molecular weight, viscoelastic, and compatible pair polymers of PVDF and PMMA. The same approach was applied to functionalized polymers to investigate the effect of physicochemical affinity on two pairs of asymmetrical reactive polymers based on PE-GMA (glycidyl methacrylate)/PVDF-*g*-MA (maleic anhydride) and a PE/PVDF as a reference. The linear viscoelastic and surface properties of the neat and bilayer model systems structures have been investigated. The optical obeservations of the encapsulation kinetic of two drops were recorded using a homemade device. Specific experiments were carried out to follow up the kinetic of encapsulation, and the results were rationalized as a function of the effect of the viscosity, elasticity ratios, drop geometry, the interfacial tension, and the physicochemical affinity. Throughout all the experiment, the mechanisms were purposed for each system and discussed based on the theories of molecular forces or Brownian motion governing diffusion and Ostwald ripening, in contrast to the theories of coalescence. The viscosity ratio coupled to the drop geometry of the material was found to be a key parameter and that it has to be linked to the interfacial tension and spreading parameters. Furthermore, the encapsulation appeared to be hindered by the interdiffusion process in the case of compatible pair system despite their elasticity and surface tension contrast. Finally, the encapsulation kinetic could be reduced or eliminated by the creation of a copolymer at the interface for a reactive system. The results obtained by the optical investigation of two drops corroborated the rheological data of the bilayer systems. Hence, the obtained results rendered it possible to decouple the influence of the viscoelastic parameters to flow, interfacial tension, thereby highlighting a number of macroscopic effects that were governed by the interdiffusion or reaction of macromolecular chains at the interface to give a better understanding of encapsulation phenomenon in multiphase systems.

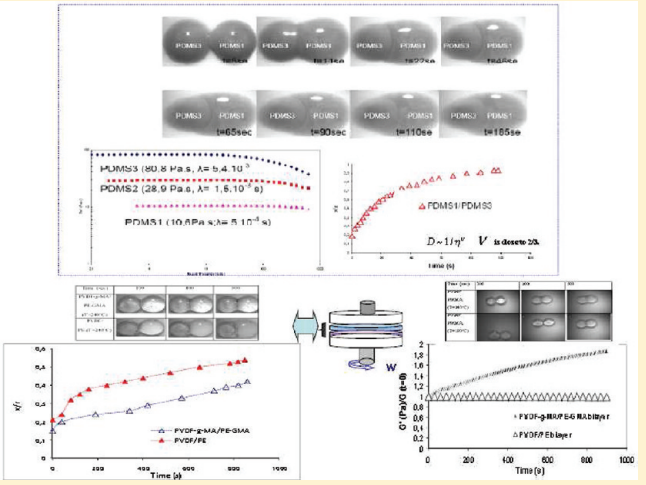

1. INTRODUCTION

Encapsulation phenomena has been observed in experiments involving a wide range of materials from oil and water to polymer melts for both high and low Reynolds numbers. It can also used as a technique in the food, biomedical, and pharmaceutical industry where small particles, cells, and cell agglomerates are produced and dispersed in an ambient medium. Encapsulation efficiency is also of primary importance in the biomedical industry, as reviewed by Orive et al.[1] The phenomenon has been also observed in other systems as in bubblesand cells.[2,3] The subject is vast, and hence it is a daunting task to summarize this remarkably rich and multifaceted area. The encapsulation subject is old in principle; the pioneering works show that lower viscosity material will eventually encapsulate the higher viscosity fluid.[4] In the case of multiphase polymer system, we shall quickly list some investigations of close relevance to the present study:

a. Encapsulation in Multilayer Structure. Previous work on layer thickness uniformity has primarily been devoted to the effects of differing polymer viscosities in the individual layers under shear.[5−9] These differences in viscosities give rise to a phenomenon known as "viscous encapsulation" in producing nonuniform layer thicknesses. There has only been performed a very limited number of experimental studies dealing with encapsulation phenomena,[10−12] and most of these research efforts

Received: May 20, 2011
Revised: September 20, 2011
Published: December 22, 2011

have suggested that, irrespective of the stability of the interface, the more viscous fluid tends to push into its less viscous counterpart, eventually leading to the less viscous fluid encapsulating the more viscous components. In other words, encapsulation is caused by the tendency of the less viscous polymer to enter the region of high shear (i.e., the wall with a highest shear stress).[13] Differences in wall adhesion and viscoelastic characteristics of polymers and weak secondary flows caused by viscoelastic effects have been demonstrated to be the contributing factors.[14] In an early study, White et al.[15] argued that the shape of the interface can also be influenced by the jump in secondary normal stress difference. Recently, it was demonstrated that this phenomenon is mainly driven by a jump in viscosity but also by a difference in elasticity between the two fluids.[16] These experimental observations are consistent with numerical studies with Newtonian and purely inelastic constitutive equations.[17,18] However, examples of coextruded structures with nonuniform layer thicknesses have been observed even when the viscoelastic properties of the materials are very similar.[19] This implies that another factor affects the flow of the materials during process. An investigation of the effect of polymer viscoelasticity and physicochemical affinity on the layer thickness uniformity of multilayer coextruded structures would thus be of great interest.

b. Encapsulation in Blend. In studies of multicomponent polymer blends of more than two phases, papers dedicated to this subject have shown that the morphology resulting from the competition between drops collision under flow followed by coalescence/encapsulation or drop breakup depends mainly on the interfacial and rheological properties.[20,21] The final droplet size distribution, under mixing, results from the balance between the present phenomena.[22] Recently, the effect of compatibilization on the deformation and breakup of drops in stepwise increasing shear flow has been investigated.[23]

Hobbs et al.[24] first reported the encapsulation concept on the spontaneous development of the composite droplet morphology in immiscible systems. They suggested that, under equilibrium mixing conditions, interfacial forces might play an important role in establishing the phase morphology of multiphase polymer blends. By using the concept of a spreading coefficient, they rewrote the Harkin equation (eq 1) in which two dissimilar phases are dispersed within a third matrix material by substituting the appropriate interfacial tensions for the surface tension values

$$\lambda_{31} = \sigma_{12} - \sigma_{31} - \sigma_{13} \quad (1)$$

Here, σ_{12}, σ_{32}, and σ_{13} are the interfacial tensions for each component pair, and λ_{31} is defined as the spreading coefficient for the case of component 3 encapsulating component 1. The index 2 refers to the matrix. λ_{31} must be positive for component 1 to be encapsulated by component 3. The authors successfully demonstrated the usefulness of the spreading coefficient concept for predicting the various morphologies that were formed and in particular the encapsulation effect.

Recently, a numerical simulation of particle encapsulation due to liquid thread breakup has been published to investigate the effect of the particle spacing, viscosity ratio, Reynolds number, and waveform of interfacial perturbations.[25]

Recent papers on ternary systems have suggested that composite droplet formation may be related to the viscosity of the dispersed components.[26] Nemirovski et al.[27] studied the phase morphology of a number of three-component (thermoplastic/thermotropic) systems and suggested that the dispersed component A would encapsulate the dispersed component B (in a matrix C) when both the thermodynamics, expressed by means of a positive $\lambda_{A/B}$ spreading coefficient, and the kinetic effects, expressed by means of a dispersed phase viscosity ratio smaller than 1, acted cooperatively. However, in some cases, a dispersed phase viscosity ratio greater than 1 was found to hinder the development of the core−shell structure (A encapsulating B) even though encapsulation had been predicted by a positive $\lambda_{A/B}$ spreading coefficient.

The reverse effect was observed by Gupta and Srinivasan[28] for ternary blends of styrene−ethylene−butylene terpolymer (SEBS) and polycarbonate (PC) dispersed within a PP matrix. The SEBS component formed a boundary layer at the surface of the PC droplets when PC was less viscous than SEBS, whereas the minor components were separately dispersed when PC was more viscous than SEBS. However, most authors have failed to find any influence of the dispersed phase core−shell viscosity ratio on the composite droplet structure.[29,48]

Recently, Reignier et al.[30] investigated the influence of the molecular weight of the dispersed phase components on encapsulation effects in the composite droplet phase for a ternary blend composed of PS and PMMA dispersed in HDPE. Hence, it was found that arguments based on the effect of viscosity ratio or the absolute viscosities of the different dispersed phases do not explain the obtained results concerning the composite droplet morphology, from PMMA encapsulating PS to PS encapsulating PMMA. This morphology depends on the molecular weight of the each polymer and the mixing and annealing times. Considering all the above, a conceptual model has been developed to predict encapsulation effects in composite droplet type systems based on the use of a dynamic interfacial tension (i.e., taking into account then elasticity of the polymer components). Calculations based on the dynamic interfacial tension model, using elasticities based on constant shear stress (first normal stress coefficient based on Laun's law), were able to account for all of the observed encapsulation effects in this work.

Finally, as briefly summarized above, significant progress in understanding the encapsulation phenomenon in multiphase systems has been obtained over the past decades. Few papers have been dedicated to polymer systems. To the best of our knowledge, few research efforts have, with regard to fundamental and experimental aspects, been dedicated to this subject. Despite the interesting nature of this kind of research, it is of no help when attempting to comprehend either the generation of the encapsulation decoupled to shear or their connection with the physicochemical affinity and viscoelasticity.

A thorough understanding of physicochemical aspects as well as of the full rheological parameters of the encapsulation phenomena has yet to be established. In order to attain this, the attention of the present study has been focused on performing original experiments with well-characterized model polymer fluids with different molar masses and functionalities. The aim of this work thus involved decoupling the influence of viscoelastic parameters and flow, thereby highlighting a number of macroscopic effects coupled to the physicochemical affinity which can affect the encapsulation phenomenon. The purpose of the investigation has been to present simples experimental studies in an attempt to gain an understanding of the mechanisms governing encapsulation decoupled to these parameters. The obtained optical results will be analyzed based on the surface properties and rheological properties of mono- and bilayer systems. The details of the experimental procedures

are presented in the next section, followed by the main results and a discussion.

2. EXPERIMENTAL SECTION

2.1. Base Materials. *a. The Model Fluids.* Three types of poly(dimethylsiloxane) (PDMS) with varying viscosities and molecular weight were chosen, and their designations and viscosities are listed in Table 1. Moreover, a complete investigation of the rheological properties of the materials was carried out.

b. High Molecular Weight Model Polymers. Two systems were kindly supplied by Arkema (Serquigny, France): (i) The first pair was based on PVDF/PMMA and was completely miscible. (ii) The second system was based on two pairs of reactive polymers at interfaces of PE-GMA (glycidyl methacrylate)/PVDF-*g*-MA (maleic anhydride). A pair consisting of PE/PVDF was used as a nonreactive system.

Table 1. Designations of the Three PDMS Materials and Their Respective Viscosities and Molecular Weights (Values Given by Sigma-Aldrich)

fluid	Newtonian viscosity (Pa·s)	M_w (g/mol)
PDMS1	10.6	76 000
PDMS2	28.9	94 000
PDMS3	80.8	130 000

Table 2. High Molecular Weight Polymers Used and Their Main Characteristics

sample code	supplier	characteristic functions	$\overline{M}_w$[a] (g/mol)	I_p[a]	T_m[b] (°C)
PVDF	Arkema	–	210 000	2	169.4
PVDF-*g*-MA	Arkema	maleic anhydride	200 000	2.2	168.5
PMMA	Arkema		195 000	1.994	120
PE	Arkema	–	240 000	9.9	114
PE-GMA	Arkema	(glycidyl methacrylate)	207 000	10	107

[a] Measured in our laboratory by gel permeation chromatography (GPC) with tetrahydrofuran (THF) as solvent for PMMA, dimethylformamide (DMF) for PVDF, and PVDF-*g*-MA and trichlorobenzene (TCB) at 135 °C for PE and PE-GMA (universal calibration). [b] Measured in our laboratory by a DSC Q20 (TA Instruments) at heating and cooling rate of 10 °C/min.

Table 2 reports all the high molecular weight polymers used in this study along with their source and some of their characteristics.

2.2. Rheological Investigations in Linear Viscoelasticity Regime. *a. Rheological Properties of the Pure Polymers.* All rheological measurements were carried out in the linear viscoelastic region in small-amplitude oscillatory shear mode as was verified by preliminary strain sweep measurements. Polymer degradation was avoided by continuously purging the oven with nitrogen. The measured rheological functions included the complex viscosity η^*, its real and imaginary components η' and η'', and the elastic modulus G' and loss modulus G'':

The rheological behavior of model fluids was studied. Flow tests were performed with a stress-controlled rotational rheometer AR100 from TA Instruments, with a cone and plate geometry (D = 60 mm, $\alpha = 2° \approx 0.035$ rad, gap = 66 μm). To obtain the largest possible range of frequencies, the tests were carried out from 25 to 65 °C. A master curve was plotted for a reference temperature of 25 °C using a time–temperature superposition procedure. Figure 1 depicts the rheological

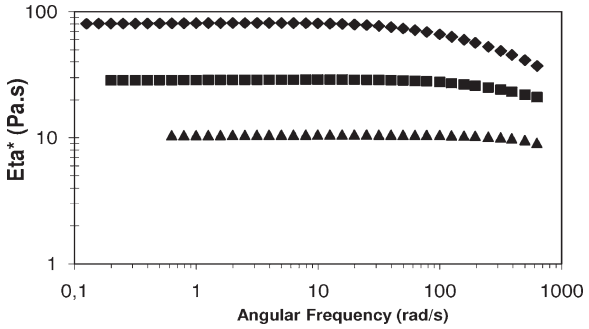

Figure 1. Complex viscosity modulus vs the frequency for PDMS1 (triangle), PDMS2 (square), and PDMS3 (diamond) at 25 °C.

Table 3. Rheological Characteristics for PDMS at 25 °C[a]

fluid	η_0 (Pa·s)	λ (s)
PDMS1	10.6	1.5×10^{-4}
PDMS2	28.9	1.5×10^{-3}
PDMS3	80.8	3.1×10^{-3}

[a] Relaxation times are calculated by the Cole–Cole method.

Table 4. Zero-Shear Viscosities η_0, Activation Energies E_a, and Relaxation Times λ for PE, PE-GMA, PVDF, PMMA, and PVDF-*g*-MA at 240 °C

polymer	η_0 (Pa·s)	E_a (kJ/mol)	λ (s)
PE	7400	53	0.9
PE-GMA	5010	56	0.79
PVDF-MA	2950	58.5	0.39
PVDF	1820	51.5	0.31
PMMA	1800	70	0.25

curves for PDMS1, PDMS2, and PDMS3. However, all polymers exhibit Newtonian behavior in the expected range of the investigation with a constant viscosity and zero first normal stress difference. Viscosity is constant, and G' is almost zero. PDMS3 does show some traces of the first normal stress difference but only at high angular frequency that are well above the maximum angular frequency used in the work. Newtonian viscosities and relaxation times at 25 °C for each fluid were then deduced from this curve (the same results have been obtained in the work of Muller et al.[31]).

Table 3 regroups these later results. Relaxation times are calculated by the Cole–Cole method. When plotting the real and imaginary parts of viscosity in the complex plan, the obtained curve presents a maximum for $\lambda\omega = 1$. We can directly deduce the value of λ. Meanwhile, the relaxation times are very small and increase with the viscosity (i.e., molar mass).

Rheological measurements for the high molecular weight polymers were performed using a strain-controlled rotational rheometer ARES (Advanced Rheometrics Expansion System, Rheometrics Co.) with a parallel plate–plate geometry. All film of PE, PE-GMA, PMMA, PVDF, and PVDF-*g*-MA were previously fabricated under identical processing conditions in order to eliminate sample-to-sample errors. All the resin granules were dried at 80 °C under vacuum to remove the moistures before use. Samples for rheological measurements were prepared by compression molding at 180 °C with a pressure of 200 bar between two Teflon films to obtain a smooth surface. During heating and cooling stages of compression, nitrogen purging was introduced to protect polymers from oxidation. All samples were prepared under the same processing conditions to eliminate samples to samples errors. These round samples were subsequently annealed at 65 °C under vacuum for 1 week to remove possible surface contaminants

dx.doi.org/10.1021/ma201151k |*Macromolecules* 2012, 45, 441–454

and to allow the relaxation of chains at the surface having become oriented as a result of shear and elongation during the film preparation.

Rheological properties were then explored within a range of temperatures spanning from 180 to 240 °C. Their master curves obtained by Arrhenius rule at a reference temperature of 240 °C. The corresponding activation energies of viscous flow calculated from the master curve at such a reference temperature are reported in Table 4.

For the sake of clarity, only the rheological results at 240 °C are presented. For example, Figure 2a confirms that PVDF and PMMA presented equivalent rheological behaviors of viscosity at 240 °C. On the basis of storage modulus values, PVDF is more elastic than PMMA at this reference temperature. In addition, Figure 2b depicts a comparison of rheological behavior (viscosity and storage modulus) of PVDF, PE, PVDF-*g*-MA, and PE-GMA at 240 °C. PMMA is not present here because it is shows the same behavior as PVDF. All the materials exhibit a Newtonian behavior at low frequencies. The viscosity curves of the PE and PE-GMA displayed a noticeable pseudoplastic behavior above 0.5 rad/s, whereas 1 rad/s for PVDF and PVDF-*g*-MA. Based on their storage modulus, PE and PE-GMA are more elastic than PVDF-*g*-MA and PVDF, respectively. This result also supported by the measurement of the first normal stress difference. These results thus confirmed that these polymers were significantly different with respect to their viscous and elastic flow properties and their high molar masses.

Table 4 summarizes also the obtained zero shear viscosities and the relaxation times calculated based on the Cole−Cole method at 240 °C. Furthermore, the comparison of the relaxations times corroborates the above obtained results based on the storage modulus. All of these studied polymers are highly viscous and elastic in comparison with PDMS.

Hence, based on these rheological investigations, the zero-shear viscosity ratios for the studied temperatures were evaluated as presented in Table 5.

b. Rheological Properties of Bilayer Systems in Linear Viscoelastic Regime. Rheological measurements of the bilayer systems (based on PVDF, PMMA, PVDF-*g*-MA, PE, and PE-GMA with symmetrical and asymmetrical configurations) were carried out under a strain-controlled rheometer: ARES (Advanced Rheometrics Expansion System) using a parallel-plate geometry (Φ = 25 mm) at different temperatures from 180 to 240 °C. Polymer degradation was avoided by continuously purging the oven with nitrogen.

The bilayer assembly for diffusion process was prepared by bringing the polymers round disks into intimate contact at room temperature with a desirable configuration before loaded between the plates and then annealed in the oven detected by a mode of the experiments. (For the sake clarity of this paper, only the experiments with dynamic time sweep test will be presented.) The zero time was defined as the time when the heating chamber of the rheometer was closed and the healing time was the contact time after having reached the plate temperature. The polymer sandwich was slightly compressed to ensure contact and obtain a desired gap. Indeed, the pressure was expected to affect the diffusion process and thus also the interpenetration of chains at the interface.

Prior experiments have been carried out by both reverse configurations, and the errors observed between the results of these two configurations were minimized through selecting a better gap between upper plate and lower plate (which is equal to the total thickness of bilayer). It is noticed that the gap was set to be equal to the total thickness of bilayer in this part of experiments is for the sake of avoiding the effects of external compression pressures, making the investigation more complicated. A prestudy was led to obtain a better gap in order to provide an improved reproducibility. Indeed, in that context, three configurations and sample thicknesses were studied: (i) 1 mm: 500 μm/500 μm; (ii) 1.2 mm: 600 μm/600 μm; (iii) 1.4 mm: 700 μm/700 μm. Nevertheless, in the present investigation, the lower viscous material was, in the case of the bilayer structure, placed close to the motor to obtain a good dissipation of strain. The most viscous material was placed at the top near the transducer. Moreover, despite reversing the position

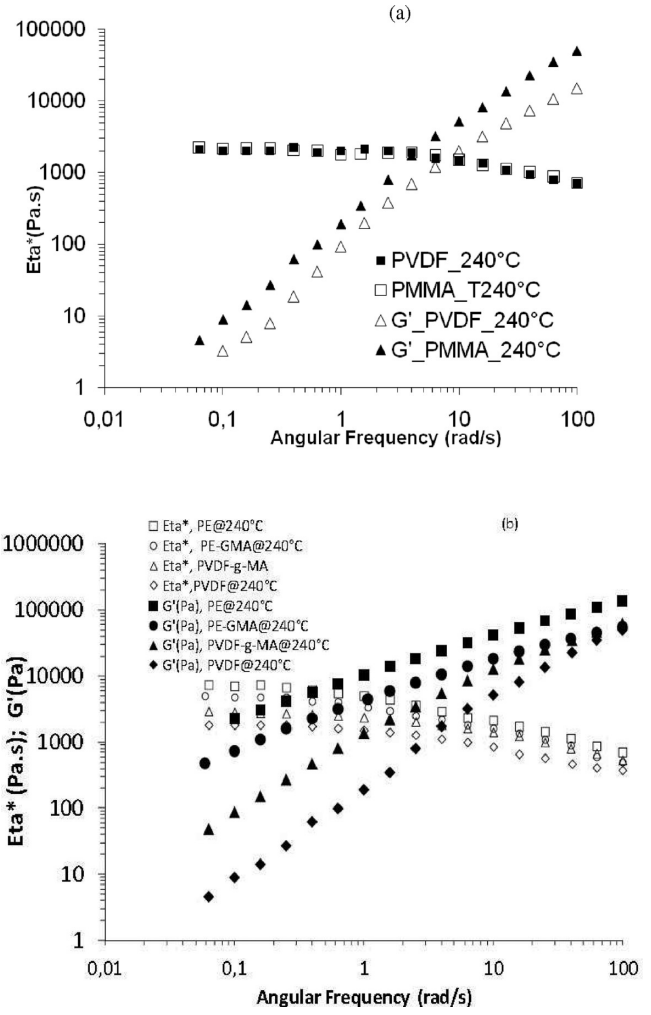

Figure 2. (a) An example of the storage and complex viscosity modulus vs the frequency of PVDF and PMMA at 240 °C. (b) Comparison of the complex viscosity modulus and storage modulus vs the angular frequency of PE, PE-GMA, PVDF, and PVDF-*g*-MA at 240 °C.

Table 5. Zero-Shear Viscosity Ratios at Different Temperatures of the the Used Polymer Pairs

	zero-shear viscosity ratio			
T (°C)	PVDF/PMMA	PE-GMA/PVDF-*g*-AM	PE/PVDF	PDMS3/PDMS1
25				8
190	1.15	2	3.8	
210	1.03	1.7	3.5	
240	1	1.5	3.2	

of the two polymer plates, equivalent results were obtained with the reactive and nonreactive systems regardless of these three thicknesses. For the sake of clarity and in order to reduce the number of samples, only the results concerning 600 μm/600 μm of bilayer are presented.

To make sure all the oscillatory measurements being performed for each configuration within the linear viscoelastic regime, a prior dynamic strain sweep test was conducted ranging from 0.1% to 100% with a maximum angular frequency (ω) amplitude of 100 rad/s. At a fixed

dx.doi.org/10.1021/ma201151k |*Macromolecules* 2012, 45, 441–454

Table 6. Surface Tension Values for Model Fluids Obtained with Three Substrates (Columns 2−4) as Well as Merely One Nonpolar Substrate (Column 6)[a]

	measurements with 3 substrates: PTFE, aluminum, and glass at 25 °C				measurements with only PTFE at 25 °C
sample	γ_L^p (mN/m)	γ_L^d (mN/m)	γ_L (mN/m)	contribution of polar part γ_L^p/γ_L (%)	γ_L^p (mN/m)
PDMS1	0.5	22.4	23.0	2.8	23.3
PDMS2	0.6	23.1	23.6	2.3	23.6
PDMS3	0.6	22.7	23.3	2.6	23.8

[a] The contribution of the polar component to the surface tension is displayed in column 5.

temperature, the dynamic time sweep tests were implemented at a 5% of fixed strain that lies in linear viscoelastic region and a given angular frequency of 1 rad/s amplitude. All measurements, whether conducted were performed with a 200 FRTN1 transducer with a lower limit of 0.02 g·cm. We considered only torques's that were 4 times higher than the lower limit of 0.02 g·cm given by the rheometer. Measurements were taken once the sample had reached a fully relaxed state and without any squeeze flow (with an axial force more than 10%). Finally, additional details of the experimental procedure can be found in previous articles of Qiu and Bousmina[32] as well as Lamnawar and Maazouz.[19,33−35]

2.3. Surface Tension Properties. The surface tension was evaluated for all samples. The contact angles between the liquids and three substrates were measured to determine the polar, γ_L^p, and the dispersive, γ_L^d, components of the liquid surface tension. When considering a liquid drop of surface tension γ_L on a solid substrate of surface tension γ_S, the equilibrium at the triple point can be written as

$$\gamma_S = \gamma_{SL} + \gamma_L \cos\alpha \quad (2)$$

where γ_{SL} is the interfacial tension between the liquid and the substrate and α is the contact angle. According to Owens and Wendt,[36] γ_{SL} can be expressed as

$$\gamma_{SL} = \gamma_S + \gamma_L - 2(\gamma_S^d\gamma_L^d)^{1/2} - 2(\gamma_S^p\gamma_L^p)^{1/2} \quad (3)$$

Taking into account eqs 2 and 3, this leads to

$$\gamma_L(1 + \cos\alpha) = 2(\gamma_S^d\gamma_L^d)^{1/2} + 2(\gamma_S^p\gamma_L^p)^{1/2} \quad (4)$$

In the above equation, the values of γ_S^d, γ_S^p, and α are known for each used substrate. This equation can be rewritten as follows:

$$\frac{1 + \cos\alpha}{2\sqrt{\gamma_S^d}} = \frac{1}{\gamma_L}\sqrt{\gamma_L^p}\sqrt{\frac{\gamma_S^p}{\gamma_S^d}} + \frac{1}{\gamma_L}\sqrt{\gamma_L^d} \quad (5)$$

By plotting

$$\frac{1 + \cos\alpha_i}{2\sqrt{\gamma_{S_i}^d}} = f\left(\sqrt{\frac{\gamma_{S_i}^p}{\gamma_{S_i}^d}}\right) \quad (6)$$

where i is the number of substrates, the polar and the dispersive components of the liquid can be easily determined from the above expressions. The obtained results are given with an average error of ±0.2 mN/m.

The surface tension can be simply estimated by

$$\gamma_L = \frac{4\gamma_S}{(1 + \cos\alpha)^2} \quad (7)$$

Table 6 summarizes the surface tension measured for model fluids on the PTFE substrate. In fact, the PTFE substrate had a surface tension γ_S of about 22.5 mN/m, and as can be seen in column 5, polar parts can be neglected. Measurements could be achieved on a single nonpolar substrate (PTFE), which improved their accuracy.

Table 7. Surface Tension Values at Several Temperatures for PE

temp (°C)	183	190	194	199	207	213	220	240
surface tension (mN/m)	22.8	22.4	21.9	21.4	20.9	20.3	20.2	19.6

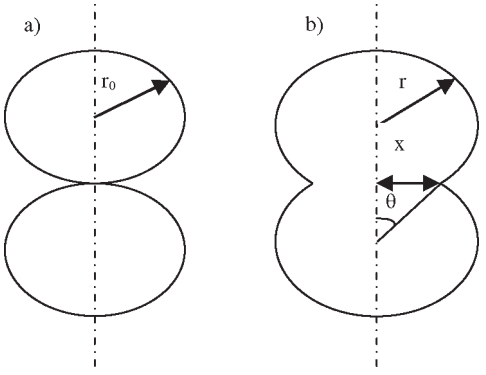

Figure 3. Geometrical illustration of the coalescence/encapsulation process of two drops at (a) $t = 0$ s and (b) $t > 0$ s. The parameters r, x, and θ represent the radius, the neck radius, and the coalescence angle, respectively.

On the other hand, the surface tension of the high molecular polymers on a PTFE substrate was calculated at each test temperature according to eq 7. A small flow of an inert gas was necessary to prevent thermal degradation of the material. As an example, Table 7 gives an example of the results obtained for PE. The surface tension varied from 22.8 mN/m at 180 °C to 19.6 mN/m at 240 °C.

The surface tension decreased linearly with the increase of the temperature with a small slope as $d\gamma/dT = -0.08$ mN/(m °C) for all studied polymers (PE, PE-GMA, PVDF, PVDF-*g*-MA, and PMMA). Similar values are found in the literature for numerous polymers and corroborate our experimental results. Indeed, Kwak et al.[37] have measured the surface tension of a PE and obtained a value of 18.3 mN/m at 240 °C. According to Wu,[38] the surface tension of a grafted PE was 20.1 mN/m at 240 °C, which was comparable to our result for PE-GMA. The values found for PVDF and PMMA, respectively 16.5 mN/m and 31.8 mN/m at 240 °C, were in agreement with those presented by Wu.[38] On the other hand, the obtained value of PVDF-*g*-MA is quietly the same as PVDF.

2.4. Optical Observations. The optical experiments were recorded on the homemade systems especially developed for this study. They were conducted on a regulated hot stage on which the drops or the particles were deposited. A Zeiss binocular and a Pantera CCD camera linked to a computer rendered it possible to record images at regular intervals. Drops were deposited on the substrate (Figure 3), and the entire process of coalescence and encapsulation was recorded. At short times, i.e., when the neck radius grew quickly, all images were analyzed.

dx.doi.org/10.1021/ma201151k |*Macromolecules* 2012, 45, 441–454

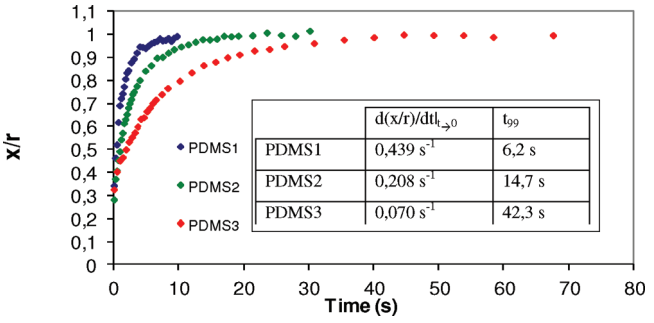

Figure 4. Coalescence/encapsulation curves for PDMS1/PDMS1, PDMS2/PDMS2, and PDMS3/PDMS3 pairs at 25 °C (r and x are the radius and neck radius, respectively).

When the encapsulation rate decreased, data were exploited every 5 or 10 images. All tests were repeated at least 3 times to ensure reproducibility. The presented results correspond to mean values of the 3 tests since this decreased the experimental error (4%).

3. RESULTS AND DISCUSSION

3.1. Primary Investigations of the Coalescence Kinetics. *a. Model Fluids.* The experiments were carried out at 25 °C for the model fluids. Only one substrate based on PTFE. To increase the contrast between the drops and the substrate, the model fluids were colored with a silicon carbide SiC powder. The amount of SiC in each fluid was ∼1%, and the size of the particles was 5 μm. The droplet size is around 8100 μm on diameter in all of measurements. (The half of this size has been used in the case of the smaller droplet in the investigation of the drop geometry effect.) Hence, the SiC particle size can be neglected compared to droplet geometry. It was experimentally verified that the addition of SiC to the fluids did not modify their rheological and interfacial properties. Drops were deposited on the substrate, and because of their low or relatively low viscosities, the fluids adopted a spherical shape more or less instantaneously. The entire process of encapsulation on 2D was recorded. At short times, i.e., when the neck radius grew rapidly, all images were analyzed.

Influence of Viscosity and the Interfacial Tension. i. Influence of Viscosity. Figure 4 compares the coalescence/encapsulation experiments for the three PDMS materials, and as can be seen, PDMS1 coalesced faster than PDMS2 and PDMS3. This was quantitatively confirmed by t_{99}, which was the time required to reach 99% of completion, and the initial slope. The experimental results corroborate those of Muller et al.[31] PDMS1 required 6.2 s to coalesce while 42.3 s was necessary for PDMS3. The initial slope also provided an indication of the encapsulation rate: from 0.439 s^{-1} for PDMS1, this value decreased to 0.070 s^{-1} for PDMS3.

The coalescence is governed by two contributions: (1) the wetting capacity and (2) the diffusion at the interface. The main driving force for particles coalescence is the surface tension, while viscous flow (according to the mobility of particles) is the opposing factor. The emphasis of lot work in the literature is on the development of a simple or general models which further could be adapted in simulating industrial process of ceramics, metals, and more complicated systems based on polymers. Frenkels models,[39] which is dedicated in the first time to metals, is based on Newtonian viscous flow under the action of surface tension. More recently, the mechanisms purposed in the literature are based on the balance of the work of surface tension and the viscous dissipation (the rate of coalescence occurring by viscous flow promoted by surface tension). All the other forces including gravity are neglected. Many authors have suggested that not only the viscous flow is acting on the coalescence but also the viscoelasticity of the material.[40] The coalescence mechanism can be explained following three steps: (1) elastic adhesive contact, (2) zipping contact growth, and (3) stretching contact. The phase 1 happens in short times. When particles are brought into contact, they deform to create a finite contact surface. The theory to describe this phase is also well-known as JKR theory.[41] The neck radius is proportional to $t^{1/3}$. The second phase (elastic driven response) occurs after the elastic adhesive contact but before the stretching contact. The neck radius growth is driven by adhesive intersurface forces and resisted by viscoelastic deformation. x/r is proportional to $t^{1/7}$. The Newtonian approach proposed by Frenkel can be used for long times. The neck radius is also proportional to $t^{1/2}$. Mazur and Plazek[42] found that the coalescence can be viewed as the sum of the elastic adhesive contact and the Newtonian contributions. Recently, Lin et al.[43] modeled sintering by adding the three contributions. They gave a good description and analysis of these three steps in their article.

In our experiments using the model polymer fluids, the observed process in the beginning times was governed by diffusion at the interface between the two drops placed in close vicinity of each other. The physical parameter responsible of interfacial tension's decreasing (i.e., compatibilization) is the interdiffusion between the neighboring phases. The theory for molecular forces or Brownian motion induced coalescence can be derived. Once the initial barrier energy was overcome (according to the interfacial energy), the two drops started to coalesce due to self-diffusion of the polymeric chains on both sides of the interface. The self-diffusion coefficient in a polymer networks is scaled as the inverse of the viscosity, $D \sim 1/\eta^{\nu}$ where the exponent ν is close to 2/3. The time of diffusion over a distance L is scaled as the inverse of the diffusion coefficient, $t = L^2/D$, and therefore increases proportionally to the viscosity $t \sim \eta^{\nu}$. For instance, PDMS3 was ∼2.8 times more viscous than PDMS2. The diffusion time in the two samples should scale with a power ν in the same proportion. An indirect way to confirm such proportionality was to compare the viscosity ratio η-(PDMS3)/η(PDMS2) with the ratio of the experimental characteristic times t_{99}(PDMS3)/t_{99}(PDMS2). Such a ratio was 2.87 for t_{99}. Similarly, the proportionality was also reasonably confirmed for PDMS2/PDMS1 and PDMS3/PDMS1.

ii. Influence of the Interfacial Tension. According to the results given in Table 6, the three values of surface tension for PDMS3 were slightly higher than for PDMS1 and PDMS2. For PDMS1, which had a low viscosity and was Newtonian, the coalescence was fast as confirmed in the last paragraph. It was possible to calculate the spreading parameter S of the fluids on the PTFE thanks to $S = \gamma_S - (\gamma_L + \gamma_{SL})$.

Table 8 gives interfacial tensions and spreading parameters for all fluids.

For $S > 0$, the wetting was complete and the fluid spread on the substrate. Contrarily, for $S < 0$, the wetting was partial, and the fluid remained a drop. For PDMS1, the spreading parameter was higher as compared to that of PDMS3 ($S = -1.34$ mN/m). The configuration was unfavorable, and the fluid had a tendency not to wet the substrate. Negative spreading parameters were also found for the other PDMS samples. PDMS1 spread better on PTFE, and a hypothesis was that the low viscosity of this fluid

dx.doi.org/10.1021/ma201151k |*Macromolecules* 2012, 45, 441–454

Table 8. Interfacial Tension of the Three PDMS Fluids on PTFE as Well as Their Spreading Parameter on PTFE

fluid	interfacial tension with PTFE (mN/m)	spreading parameter on PTFE (mN/m)
PDMS1	8×10^{-3}	−0.84
PDMS2	1.2×10^{-2}	−1.06
PDMS3	1.9×10^{-2}	−1.34

allowed a faster spreading and coalescence as opposed to for PDMS3.

The present results can also explained based on the theories of Ostwald ripening which predict a decrease in the droplet growth rate with increasing interfacial tension in contrast to the theories of coalescence.[40,44] In the literature, Ostwald ripening is a physical process in which molecules from a droplet diffuse into other phase (matrix in blend for example) due to the differences in capillary pressures between large and small droplet. Meanwhile, the calculation of the spreading parameters based on the surface tension measurements show that this parameter was higher for PDMS1 compared to PDMS2 and PDMS3 even its lower viscosity. Note that S is also negative for the three PDMS.

The Ostwald ripening predicts a decrease on the droplet growth rate with a higher interfacial tension:[44] $[\gamma_{PDMS3} > \gamma_{PDMS2} > \gamma_{PDMS1}] \Rightarrow [S_{PDMS1} > S_{PDMS2} > S_{PDMS3}]$). Indeed, PDMS1 coalescence faster than PDMS2 and PDMS3, respectively $(d(x/r)/dt|_{t\to 0} = 0.439\ s^{-1}$ for PDMS1 compared to $d(x/r)/dt|_{t\to 0} = 0.07\ s^{-1}$ for PDMS3). For PDMS3, the wetting is unfavorable, and the diffusion is slowed down because of its high viscosity. For PDMS 1, for example, despite a negative spreading parameter, the diffusion is higher and this effect seems not to be affected by a low wetting capacity.

In fact, t_{99} evaluated in Figure 4 can be reduced in order to take into account the zero-shear viscosity, the surface tension, and the initial particle radius: $t_r = t_{99}\gamma/\eta_0 r_0$. They are respectively 3.15, 3.03, and 3.09 for the PDMS1, PDMS2, and PDMS3. The calculated values are similar for the three polymers on the same substrate. This indicates that the viscosity, surface tension, and the droplet geometry radii play a combined role. Furthermore, we can scale also the graphs with dimensionless time of Pokluda et al.[45] given by $t\gamma/\eta r_0$where γ is the surface tension and r_0 and η are the initial particle and the viscosity, respectively. However, on the contrary of our in which we have taken into account the real radius versus time (it was evaluated in situ with our special optical device), Pokluda et al.[45] assumed as Frenken that the particle radius is constant $[r(t) = r_0]$ and made an approximation for small angles $\cos(\theta) = 1 - (\theta^2/2)$. In our case, only the second assumption is taken into account. The work is in progress to modeless with numerical simulation this phenomenon, and this dimensionless time to verify the limits of Frenkel, Belluhumeur, and Pokluda models.

Furthermore, the effect of surface tension is highlighted through this investigation and should be taken into account especially for the high viscous materials. The interfacial tension plays a role for the more viscous materials at a same temperature and may accelerate or slow down the kinetics depending on the wetting of the substrate (i.e., spreading parameter). Hence, the effect of the viscous forces than initially supposed was more complex and should be coupled to the interfacial forces.

b. High Molecular Weight Polymers. The optical observations of the high molecular polymers were performed on the PTFE substrate at a variety of temperatures ranging from 180 to 240 °C. All of the measurements were carried out under nitrogen to avoid degradation. Similar to the model fluids, the spreading parameters seemed to be $S < 0$. Hence, theses investigations rendered it possible to examine the effects of viscosities, relaxation times, and interfacial reaction in the case of the reactive system. For the sake of clarity, all of these results are discussed in the next paragraph.

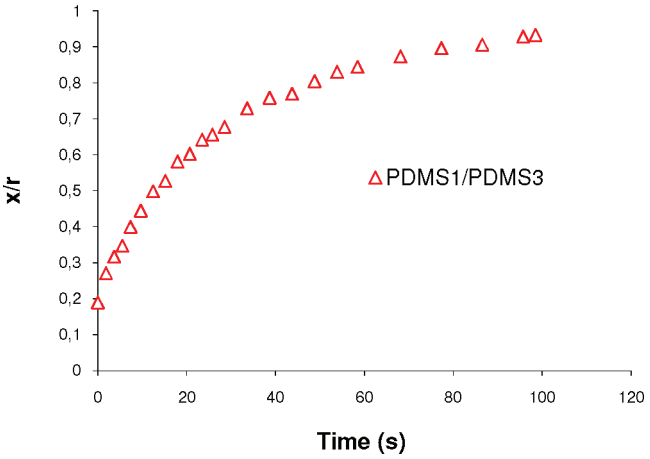

Figure 5. A coalescence/encapsulation curve of PDMS1/PDMS3 drops at 25 °C (r and x are the radius and neck radius, respectively).

3.2. Highlights of the Encapsulation Kinetics of the Model Fluids. *a. Influence of the Viscosity Ratio and the Surface Tension.* The encapsulation phenomenon was recorded by optical observations as a function of the viscosity ratio and the polymer/substrate interfacial tension. The relaxation times of PDMS are smaller and can be neglected. Figure 5 displays an illustration of the coalescence evolution of the PDMS1/PDMS3 pair, for which the viscosity ratio reached a value of 8. As symmetrical polymers, the first step of the observed encapsulation process was governed by diffusion at the interface between the two drops placed in close vicinity of each other. The theory for molecular forces or Brownian motion induced coalescence can be derived. Once the initial barrier energy was overcome, the two drops started to coalesce due to self-diffusion of the polymeric chains on both sides of the interface. Moreover, the relaxation times of PDMS(s) are neglected. In addition, it should be kept in mind that the interfacial tension of PDMS1 and PDMS3 with the PTFE substrate was 8×10^{-3} and 1.2×10^{-2} mN/m, respectively. PDMS1 spread better than PDMS3 because it is higher spreading parameter. The calculation of capillary number $Ca = \sigma R/\gamma_{12} = \eta\dot{\gamma}/(\gamma_{12}/R)$, which represents the ratio between viscous stresses (shear for example), $\sigma = \eta\dot{\gamma}$, that tend to deform the drops and interfacial stresses, γ_{12}/R, that resist to the deformation and tend to restore the initial shape of the drop, R being the drop radius and γ_{12} the interfacial tension. Indeed, the capillary numbers calculated (at lower shear rate $\dot{\gamma} = 1\ s^{-1}$, for example) are as follows: $Ca_{PDMS1} = 10.6/1.97 \Rightarrow 10.6 \gg 1.97$; $Ca_{PDMS3} = 80.8/4.68 \Rightarrow 80.8 \gg 4.68$. Considering PDMS3 as a matrix: $Ca_{PDMS1\to PDMS3} = 80.8/7.4 \times 10^{-1} \Rightarrow 80.8 \gg 7.4 \times 10^{-1}$. The PDMS1/PDMS3 interfacial tension $(= 3 \times 10^{-3}$ mN/m) was calculated using the generic-mean equation given in ref 38 from the surface tension values given in Table 7 and neglecting the polar interaction. Hence, the viscous forces appeared to be very higher in comparison to their capillary counterparts.

dx.doi.org/10.1021/ma201151k |*Macromolecules* 2012, 45, 441–454

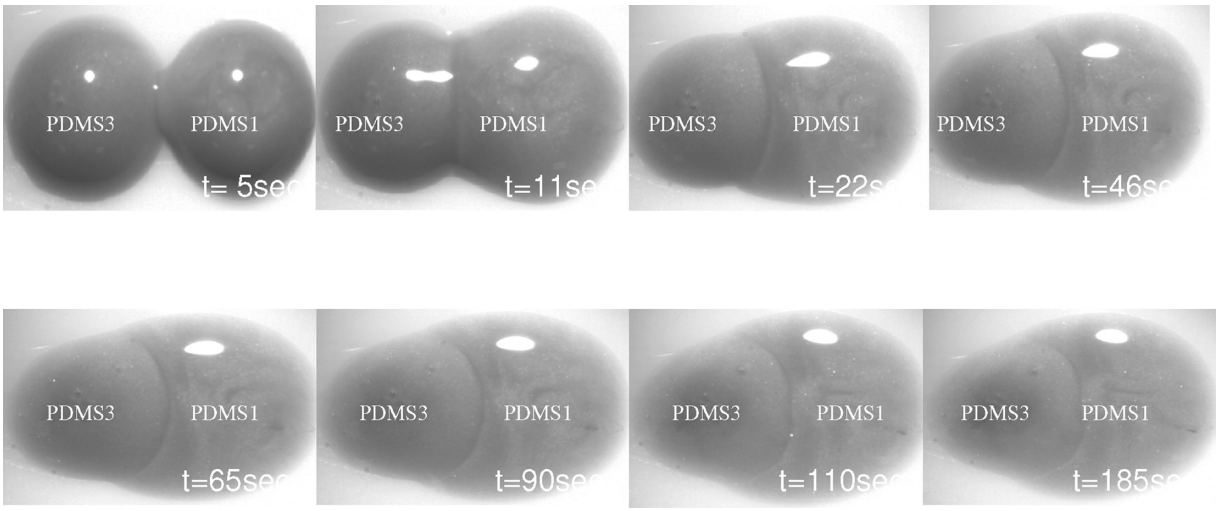

Figure 6. An illustration of the encapsulation at 25 °C in the case of the PDMS1/PDMS3 pair.

Furthermore, Figure 6 provides an experimental illustration of the fact that the less viscous polymer tended to encapsulate its more viscous counterpart but at a low shear rate.

We remind that the digital image analysis software was used to analyze the obtained pictures. A neck radius x can be calculated in situ by our special optical device and mathematical program. Images of neck growth evolution were taken as a function of time to obtain the dimensionless neck radius (x/r), where x is the length of the neck between the two particles and r is the mean radius of the droplet. In the short time, when the neck radius grew quickly, all images were analyzed. It is get of easy process. When the encapsulation is more pronounced, a special tool in the Matlab program is developed here to evaluate with accuracy the boundary between the two drops and also the real angle θ. At longer time, it is difficult to provide a clear distinction of the thinner neck radius; a lot of experiments have been carried out and repeated to have a reproduction of the measurements. These details are included in the text.

To illustrate this phenomenon, the initial encapsulation strain rate between t_1 and t_2 can be calculated from the results of Figure 4 by

$$\dot{\varepsilon}_i = \frac{x_2 - x_1}{x_2} \frac{1}{t_2 - t_1} \tag{8}$$

The initial strain rate between two times can be calculated. x_1 and x_2 are respectively the neck radius at t_1 and t_2, respectively. It appeared that $\dot{\varepsilon}_i$ was 0.07 and 0.43 s^{-1} for PDMS3 and PDMS1, respectively.

According to Frenkel, the strain rate is assumed to be constant throughout the complete domain. The obtained lower values of $\dot{\varepsilon}_i$ in our experiments allowed us to confirm that the observed encapsulation proven also at low strain and stress rate. In the literature of coextrusion process, a lot of papers accord this phenomenon only to the effect of higher shear rate in which the lower viscous polymer is forced to encapsulate the higher viscous one (viscous dissipation). The obtained results confirmed that this phenomenon is not the sole mechanism; it is shown here, experimentally, that encapsulation can occur at low shear or strain rate, and it is governed by surface and viscous forces.

Moreover, the higher viscosity ratio between PDMS3 and PDMS1 seems to be the principal parameter and the motor of the encapsulation phenomena (confirmed previously by the calculated *Ca* number: viscous forces are very higher compared to capillary forces). For the clarity purpose of our paper, only the experiments of PDMS1/PDMS3 are presented. The same conclusions were noted in the experiment observations of PDMS1/PDMS2 and PDMS2/PDMS1 couples.

b. Influence of Drop Geometry. Figure 7 illustrates the role of the drop geometry in the kinetics of encapsulation of model fluids. PDMS3 was chosen to investigate the role of the drop geometry. The encapsulation kinetics were recorded with two drops of different shape (the diameter of the smaller drop is one-half of the bigger one) (Figure 8), and their kinetics were compared to the PDMS3/PDMS3 evolution with identical drops. The slow kinetics of the (x/r) evolution could be noted with PDMS3/PDMS3 using a different drop shape.

We aware that it is very difficult to find, in the first times, if there is encapsulation of small droplet by the bigger one. However, a special numerical program using Matlab allowing finding the real boundary and distinction between two drops observed by the polarized microscope coupled to the CCD camera. It is important to note that the concentration of SiC was varied in each drop to make a clear distinction between drops. We have also thanked to use a pigment colorant for each drops, but it is too difficult to choose a suitable miscible colorant which cannot change the rheological behavior and the surface tension properties.

In conclusion, these simple experiments provided an illustration to the fact that the drop geometry was also a key parameter that needed to be taken into account. At a small shear rate, the small drop was encapsulated by the bigger one. When the drops had the same geometry, a high surface contact area interfacial area/volume allowed the chains to diffuse, thus increasing the density across the interface/interphase.

This was quantitatively confirmed with the parameter t_{99}. PDMS3/PDMS3 drops of equal shape required 42.3 s to coalesce while 140 s was necessary for the second system. However, the initial slope was quite similar for both of the studied systems (0.07 s^{-1} for the first as compared to 0.067 s^{-1} for the second).

3.3. Experimental Investigation of the Encapsulation Phenomenon of High Molecular Weight Model Polymers. *a. Effect of Elasticity and Interfacial Tension.* In order to investigate

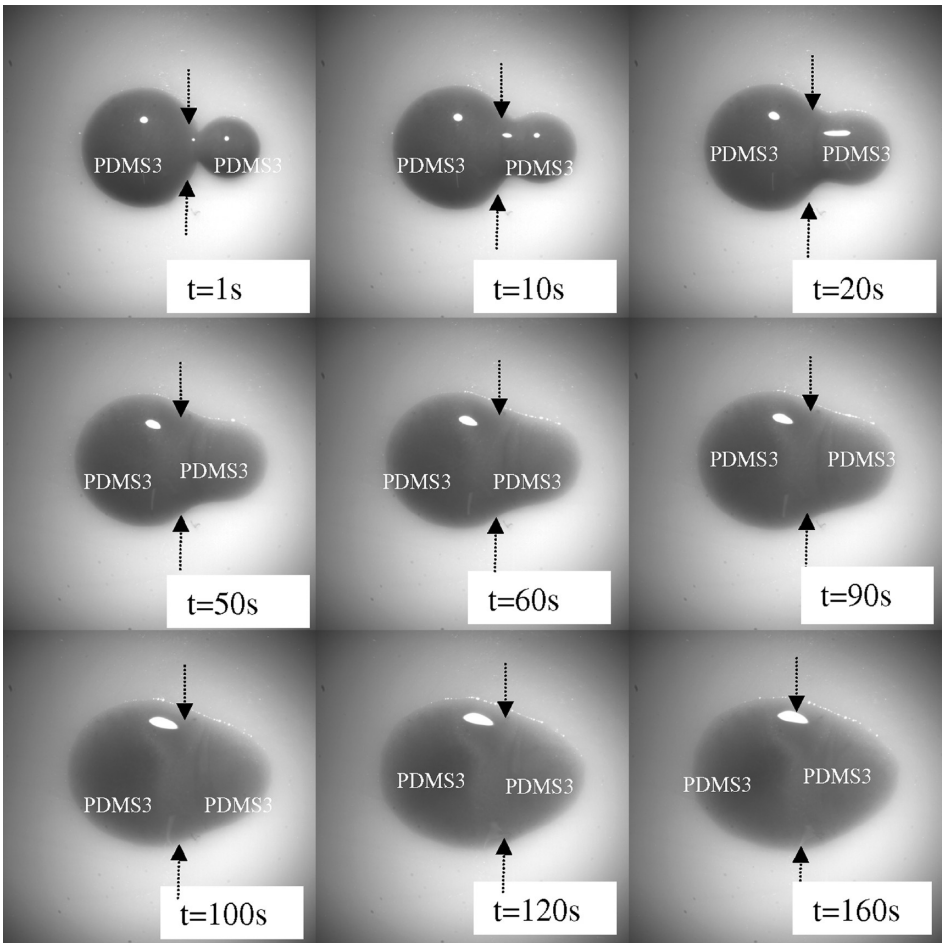

Figure 7. An illustration of the encapsulation at 25 °C in the case of two PDMS3/PDMS3 pairs differing in geometry.

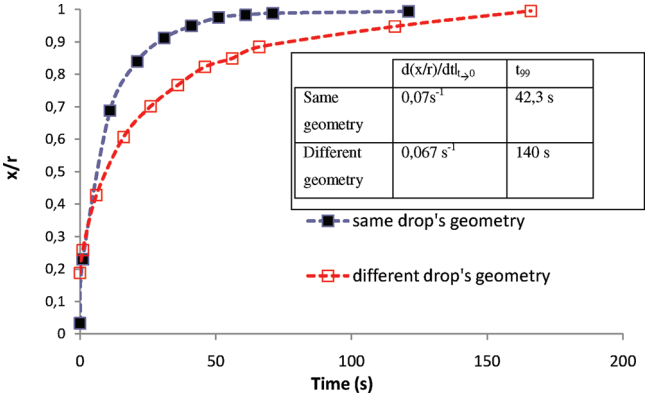

Figure 8. Influence of the drop geometry effect on the PDMS3/PDMS3 encapsulation phenomenon at 25 °C (r and x are the radius and neck radius, respectively).

the effect of the elasticity and interfacial tension on the encapsulation phenomenon, studies were performed on completely miscible, high molecular materials based on PVDF/PMMA which they present close viscosities. Poly(vinylidene fluoride) (PVDF)/poly(methyl methacrylate) (PMMA) multiphase systems, as an example of crystalline/amorphous polymers, are miscible in the molten state. Furthermore, and according to their rheological behavior, the chosen materials present the same viscosity ratio especially at 240 °C. The following investigation allows us also to probe the effect of elasticity and interfacial tension on the encapsulation kinetic.

Numerous studies of this blend have been carried out from scientific and technological view points. The miscibility of PVDF/PMMA couple is thought to be the result of an interaction between oxygen and carboxyl groups of PMMA and hydrogen atom of PVDF. Their lower Flory−Huggins parameter confirmed this purpose ($\chi \cong -0.07$).[46,47]

Furthermore, the kinetic of coalescence was assessed at several temperatures and the comparison between the encapsulation kinetics of PVDF/PVDF, PMMA/PMMA, and PVDF/PMMA are given in Figure 9a,b.

Meanwhile, it is important to note that the radius of drops is calculated here in situ with time, and it is not constant on the contrary of the assumptions of Frenkel. The different curves given the x/r versus time do not start at the same x/r. First of all, even that all images are treated, not all the points are in the represented in the plotted figures for the clarity purpose and to make distinction when we compare the kinetics in the beginning times. Moreover, the difference is around 0.05 in the majority of measurements. This is an experimental error because it was too difficult to prepare the same drops with identical size (r = 4054 μm). The granulate diameter can be varied slightly in the preparation of high molecular weight polymer or with 2D wetting

dx.doi.org/10.1021/ma201151k |*Macromolecules* 2012, 45, 441–454

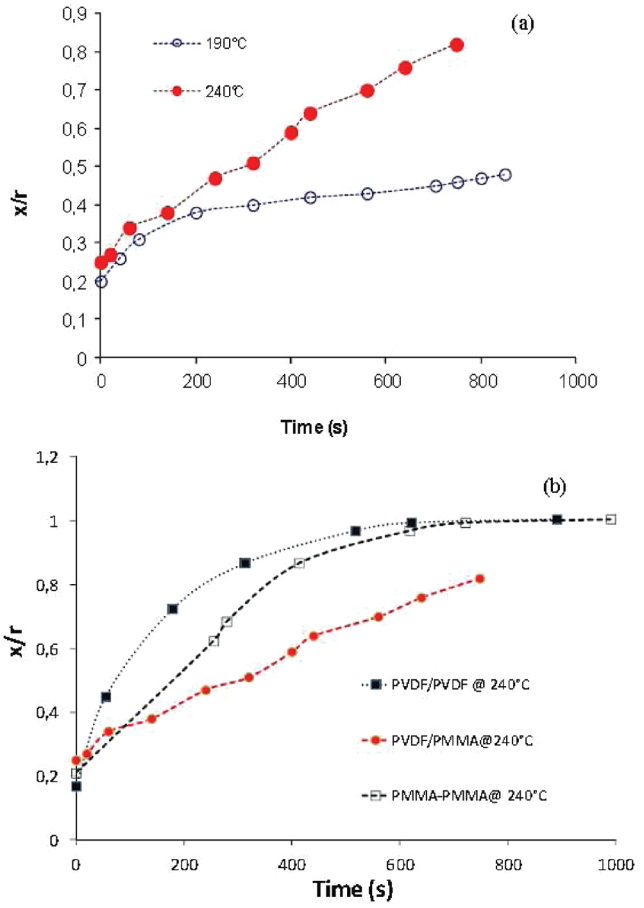

Figure 9. (a) Encapsulation kinetic curves of PVDF/PMMA drops at 190 and 240 °C (r and x are the radius and neck radius, respectively). (b) Comparison of the encapsulation kinetics at 240 °C between PVDF/PVDF, PMMA/PMMA, and PVDF/PMMA.

on the PTFE substrate of PDMS depending on their spreading parameter. This small difference in the initial size does not affect any way the kinetics of encapsulation, and the radius and neck radius are calculated with accuracy.

As reported in the rheological part, both of PVDF and PMMA are more viscous at 190 °C compared to 240 °C. We note that the kinetic of coalescence in Figure 9a is slower at 190 °C. The faster kinetics at this higher temperature is attributed to higher mobility of chains which can be represented by the lower viscosity. The coalescence at the 240 °C is nearly complete (x/r = 0.9) compared to 190 °C.

In this part dedicated to high molecular polymers based on PVDF and PMMA, it is of the interesting case which the materials have a close viscosity and the contrast of elasticity and the surface tension with PTFE We remind that the viscosity ratio is close to 1 despite the increasing of temperature from 190 to 240 °C (from 1.15 to 1, respectively). The only discriminating parameter between these two fluids which is not taken into account in the reduced time (t_r) is their elasticity.

Figure 9b shows that the PVDF/PMMA coalescence kinetics is less pronounced as compared to those of PVDF/PVDF and PMMA/PMMA. The relaxation times are respectively 0.31 and 0.25 s for PMMA and PVDF. They are more elastic compared to PDMS. The values of interfacial tension of PVDF and PMMA with PTFE are 16.5 and 31.8 mN/m at 240 °C, respectively. This large difference of interfacial tension has also a role here. The spreading parameter of PVDF is then more higher compared to PMMA. They are also negative allowing the partially wetting PDMS and to not accelerate the coalescence. However, they coalescence totally and their x/r reach the value x/r = 1.

Despite the close viscosities of the two materials, it is clearly shown here that driving interfacial forces can be counterparts by the elastic forces according to the higher relaxation times of PVDF and PMMA, respectively.

Muller et al.[31] observed an increase of the elasticity lead to an increase of the reduced time in the case of Boger fluids. Indeed, it appears that the higher interfacial tension and relaxation time of PVDF and PMMA attenuated the rate of coalescence as it was confirmed experimentally of PMMA/PMMA in comparison with PVDF/PVDF system. It is too surprising also that the calculated t_{99} are very close for the two couples even the lower kinetic coalescence of PMMA/PMMA. The corresponding x/r reaches the value 1 beyond 600 s even though the coalescence rate of PMMA/PMMA is less than PVDF/PVDF before this time. The lower relaxation time (i.e., elasticity) of PMMA seems to be the principal parameter at longer time which can explain the counterbalance of its higher interfacial tension.

In addition, PVDF/PMMA represents the lower coalescence kinetics, and its t_{99} is much longer than those of PVDF/PVDF and PMMA/PMMA. Furthermore, no encapsulation phenomenon could be seen in the different experimental conditions as demonstrated by Figure 10, despite the difference in elasticity and surface tension.

The observed development represented the signature of the kinetics of diffusion where the macromolecular chains intertwined and gradually became replaced by a more robust interphase. This result can be explained on the basis of the diffusion mechanism which was significant in the case of symmetrical polymer/polymer interface. The encapsulation appeared to be hindered by the interdiffusion process in the case of miscible pair system despite their elasticity and surface tension contrast. In conclusion, the viscosity ratio seems to be a motor of encapsulation mechanism, and its role is very complicated and should be coupled to the elasticity and interfacial tension.

Furthermore, the results from an optical investigation of the coalescence kinetics of two drops corroborated those obtained through rheology of the bilayer systems according to the procedure given in our previous work in the PE/PA6 reactive pair system. For the sake of clarity, additional details of the experimental procedure can be found in previous articles of Qiu and Bousmina[32] as well as Lamnawar and Maazouz.[19,33−35]

In the present work, the rheological measurements were carried out under small amplitude of deformations (linear viscoelastic region) to rule out the effect of flow brought by large deformation on the diffusion process, to obtain the linear viscoelastic region; a prior dynamic strain sweep test was accomplished. The strain amplitude was chosen (5%).

An example of the evolution of G' and $G'(t)/G'(0)$ of bilayer with healing time at 190 and 240 °C is depicted in Figure 11. The noticeable G' increment of bilayer with time is attributed to the diffusion process taking place at the polymer−polymer interface. The present interface will be replaced by the robust interphase between the neighboring layers according to the mutual diffusion of chains. For more clarity, the increment with time is disposed in a form of $G'(t)/G'(0)$ compared with neat polymers, where the near linearity of $G'(t)/G'(0)$ to 1.0 of the neat polymers through the whole measuring time indicates their stability at the

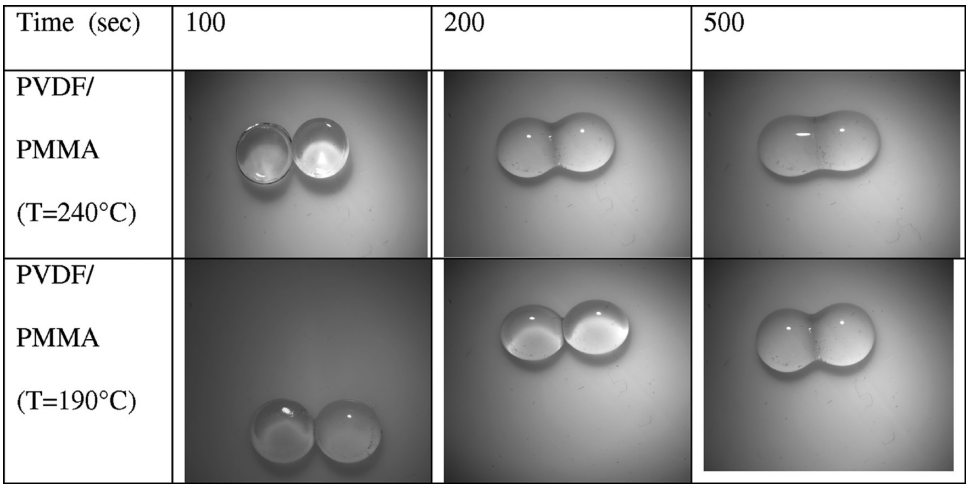

Figure 10. Illustration of the coalescence/encapsulation kinetics of PVDF/PMMA drops at 190 and 240 °C.

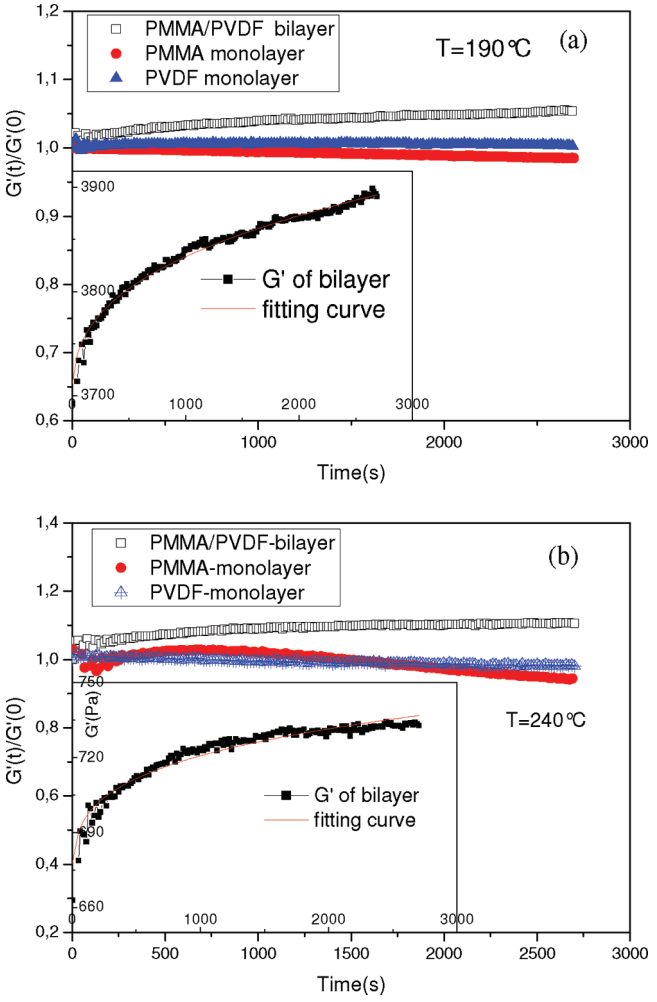

Figure 11. Evolution of G' and $G'(t)/G'(0)$ of PVDF/PMMA bilayer with healing time and corresponding fit curve at ω = 1 rad/s under different temperatures: (a) 190 °C; (b) 240 °C.

temperature measuring. The increase in storage modulus is a signature of the diffusion processes across the interface. As the mass transport proceeds, the initial weak interface strengthens

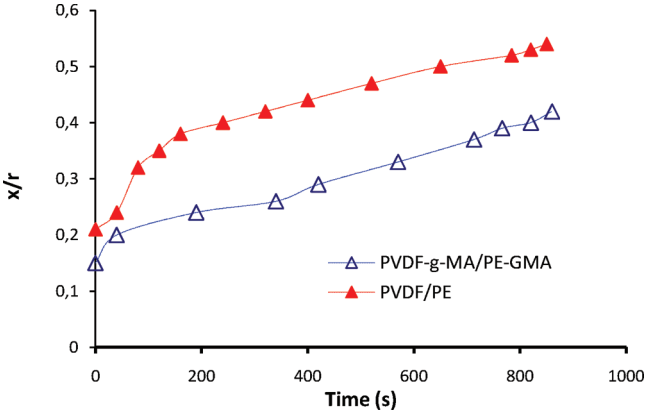

Figure 12. Comparison of encapsulation curves at 240 °C featuring PVDF-*g*-AM/PE-GMA and PVDF/PE drop systems (r and x are the radius and neck radius, respectively).

with time due to the interpenetration of polymer chains that are continuously delivered by the polymer bulk reservoirs of the two sides of the interface. Hence, the kinetics of diffusion is very fast at 240 °C compared to 190 °C according to the increase of chains mobility with temperature.

In conclusion, the rheological investigation confirmed that the kinetic of diffusion can be followed and demonstrated with the increasing of storage modulus. This observation is corroborated with optical observations which the slop of the neck radius increase significantly at 240 °C according to higher mobility of chains and the decreasing of the relaxation time compared to 190 °C. Hence, we can note a perfect ad equation between rheological and optical observations.

b. Effect of Chemical Compatibilization. Moreover, the same approach was applied to functionalized polymers in order to investigate the effect of reactive compatibilization on the encapsulation phenomenon. Two pairs of reactive polymers at interfaces based on PE-GMA (glycidyl methacrylate)/PVDF-*g*-MA (maleic anhydride) as well as a nonreactive material at an interface based on PVDF/PE were selected. The kinetics of coalescence were evaluated at several temperatures. For example, Figure 12 shows a comparison of the encapsulation kinetics of these systems at 240 °C.

dx.doi.org/10.1021/ma201151k |*Macromolecules* 2012, 45, 441–454

The interfacial reaction between MA and GMA functions certainly attenuated the coalescence kinetics.

As shown in Figure 2, the viscosities of PE-GMA are smaller than PE. On the contrary, this of PVDF-*g*-MA is more higher compared to PVDF. Meanwhile, it is also important to note that the viscosity ratio of PE-GMA/PVDF-*g*-MA is lower compared to PE/PVDF, allowing a higher mobility of chains before reaction (diffusion-controlled reaction mechanisms). Furthermore, results from an optical investigation of the coalescence kinetics of two drops corroborated those obtained through rheology of the bilayer systems. Indeed, the observed phenomena and the results can be analyzed based on the physicochemical mechanisms involved in the diffusion/reaction interfaces. As can be seen from Figure 13, the elastic modulus of PE-GMA/PVDF-*g*-MA increased with time as compared to the nonreactive system based on PE/PVDF. In fact, no significant increase in viscosity was found in the case of the latter, thus confirming that the observed phenomenon was caused by the reactivity at the interface at a low oscillation frequency.

In addition, the viscosity ratio at 240 °C of PE/PVDF is much higher compared to PE-GMA/PVDF-MA. It is decreased to 1.5 from 3.2 (half that of the nonreactive system). Note that the reactive system stay having a higher viscosity ratio, but this value is more close to 1 than this of the nonreactive system. The lower viscosities of functionalized polymer allow a higher mobility of chains to move for reaction (diffusion-controlled reaction).

Since a reactive polymer bilayer generates graft or block copolymers near the interface, each block (or graft) component can easily entangle with (or stick to) the corresponding homopolymer located near the interface. Thus, such an interface should be strengthened as compared to an interface without graft or block copolymers. This could increase the viscosity of the reactive polymer bilayer as opposed to that of a nonreactive polymer bilayer. Consequently, such a behavior was evidence of the formation of a copolymer from the reaction of PE-GMA and the carboxylic and maleic anhydride functions of functionalized PVDF.

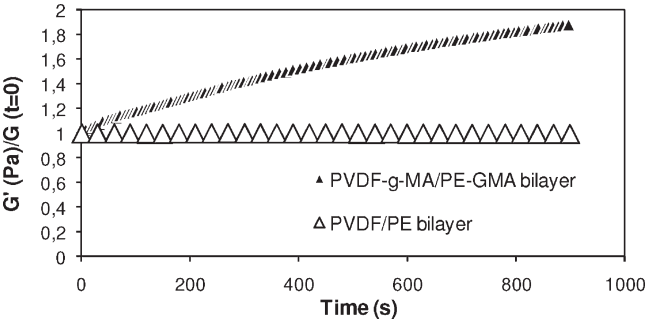

Figure 13. Comparison of the evolution of $G'(\mathrm{Pa})/G'(t=0)$ vs time at 240 °C for a reactive bilayer PE-GMA/PVDF-*g* system and a nonreactive one based on PE/PVDF.

Finally, no encapsulation was noted in these cases despite that the zero shear viscosity ratio of PE-GMA/PVDF-*g* MA was close to 1.5 (Figure 14). The triggered copolymer at the interface hinders the encapsulation kinetic. On the contrary, the nonreactive system as PE/PVDF with a higher viscosity ratio (close 3.2) confirms that the PVDF tend to encapsulate the PE. This reaction was confirmed by the rheological tool, and no encapsulation between the reactive drops is noted at this temperature on the contrary of PE/PVDF pair.

This seemed to confirm that it was essential to couple the viscosity ratio to the physicochemical affinity and viscoelastic parameters in order to gain a better understanding of the encapsulation phenomenon in multiphase systems. In addition, the role of the viscosity ratio, elasticity ratio, and layer ratio should also be investigated, thereby coupling to the reaction rate/compatibilization phenomena of the polymer/polymer interface. Indeed, for a reactive system, the encapsulation phenomenon could be reduced or eliminated by the creation of a copolymer at the interface. Finally, this system is more complex which it is essential to couple the role of viscoelasticity and the physicochemical affinity. More investigations are in progress to decouple the role of these parameters.

4. CONCLUSIONS

Throughout the investigation, the encapsulation phenomenon was recorded by optical observations as a function of the viscosity ratio, elasticity, and the polymer/substrate interfacial tension. All the experiments are conducted on a PTFE substrate. The effects of viscosity, surface tension, and relaxation time are highlighted. The model experiments do not require any labeling, and the spirit here is based on the decoupling between flow or shear and the physical parameters.

1. The investigation of model Newtonian polymers based on poly(dimethylsiloxane) of varying molar masses showed that the viscosity ratio of the material was a key parameter and that it had a considerable influence on the kinetic of encapsulation phenomenon. The used polymers are fluids at room temperature. One can perfectly control their rheological behavior and surface tension. The coalescence experiments are conducted on a PTFE substrate. The encapsulation of two drops or molten particles placed in close vicinity of each other was monitored with a CCD camera at regular intervals time. An experimental illustration was

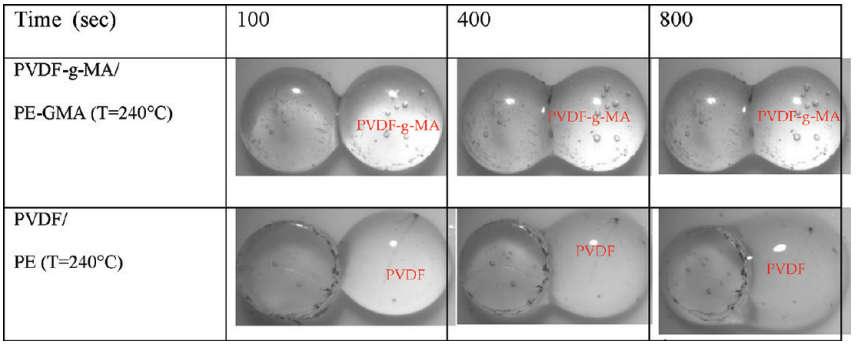

Figure 14. Illustration of the encapsulation kinetics of PVDF-*g*-MA/PE-GMA and PVDF/PE drops at 240 °C.

given to confirm that the less viscous polymer tended to encapsulate its more viscous counterpart but at low strain and shear rate. Throughout all the experiment, the mechanisms were purposed for each system and discussed based on the theories of molecular forces or Brownian motion governing diffusion at the polymer polymer interfaces. Furthermore, the effect of surface tension is highlighted through this investigation and should be taken into account especially for the high viscous materials. The interfacial tension played a role for the more viscous materials at the same temperature and was found to accelerate or slow down the kinetics depending on the spreading parameters. The results can also explained based on the theories of Ostwald ripening which predict a decrease in the droplet growth rate with increasing interfacial tension in contrast to the theories of coalescence. We demonstrated that the encapsulation phenomenon for these model fluids governed by two contributions: (i) the wetting capacity and (ii) the diffusion at the interface.

On the other hand, this work showed that the viscosity ratio coupled to drop geometry and of the material was a key parameter and that it had a considerable influence on the encapsulation kinetics. At a low shear rate, the small drop was encapsulated by the bigger one. A high surface contact/volume allowed the chains to diffuse, thus increasing the density across the interface/interphase. Meanwhile, these results also confirmed that the viscous dissipation mechanism (encapsulation at high shear rate) given in the literature was not the sole mechanism present to explain the phenomenon. On the basis of these results, we demonstrate that the viscosity ratio seems to be a motor of encapsulation mechanism, and its role is very complicated and should be coupled to the elasticity and interfacial tension.

2. In a second step, the kinetics of encapsulation of the high molecular weight based on PVDF/PMMA were assessed at several temperatures and compared to the corresponding results for PVDF/PVDF and PMMA/PMMA used as references. The present asymmetric, viscoelastic system is completely compatible and fully characterized. PVDF and PMMA have the same viscosity behavior. Indeed, the effect of elasticity and interfacial tension was highlighted. Furthermore, no encapsulation phenomenon was seen despite the difference in elasticity and surface tension for PVDF/PMMA with the same viscosity as compared to the symmetrical references. The encapsulation appeared to be hindered by the interdiffusion process in the case of compatible pair system despite their elasticity and surface tension contrast. The observed development represented the signature of the kinetics of diffusion where the macromolecular chains intertwined and gradually became replaced by a more robust interphase. The present phenomenon has been confirmed by the rheological investigation of the present bilayer systems.

3. Finally, the same approach was applied to functionalized polymers. Two pairs of reactive polymers at interfaces based on PE-GMA (glycidyl methacrylate)/PVDF-*g*-MA (maleic anhydride) as well as a nonreactive material at an interface based on PE/PVDF were selected.

In addition, the viscosity ratio at 240 °C of PE/PVDF is much higher compared to PE-GMA/PVDF-MA. It is decreased to 1.5 from 3.2 (half that of the nonreactive system). Note that the reactive system stay having a higher viscosity ratio, but this value is more close to 1 than this of the nonreactive system. The lower viscosities of functionalized polymer allow a higher mobility of chains to move for reaction (diffusion-controlled reaction). This reaction was confirmed by the rheological tool, and no encapsulation between the reactive drops is noted at this temperature on the contrary of PE/PVDF pair. The triggered copolymer at the interface hinders the encapsulation kinetic. On the contrary, PE/PVDF with a higher viscosity ratio (close 3.2) confirms that the PVDF tend to encapsulate the PE. The results obtained by an optical investigation of the encapsulation kinetics of two drops corroborated rheological data of the bilayer systems. The observed phenomena and the results were analyzed based on the physicochemical mechanisms involved in the diffusion/reaction interfaces. This seemed to confirm that the parameter should be coupled to the physicochemical affinity and viscoelastic parameters in order to give a better understanding of encapsulation phenomenon in multiphase systems. Meanwhile, the present system is more complex which it is essential to couple the role of viscoelasticity and the physicochemical affinity. More investigations are in progress to decouple the role of these parameters. Finally, the role of the viscosity ratio, elasticity ratio, and the interfacial tension should also be investigated, thereby coupling to the reaction rate/compatibilization phenomenon at the polymer/polymer interface. Indeed, for a reactive system, the encapsulation defect could be reduced or eliminated by the creation of a copolymer at the interface.

Hence, the obtained results rendered it possible to decouple the influence of the viscoelastic parameters to flow, interfacial tension, thereby highlighting a number of macroscopic effects that were governed by the interdiffusion or reaction of macromolecular chains at the interface to give a better understanding of encapsulation phenomenon in multiphase systems.

AUTHOR INFORMATION

Corresponding Author

*E-mail: abderrahim.maazouz@insa-lyon.fr (A.M.).

ACKNOWLEDGMENT

The authors express their appreciation to the reviewers for their constructive and meticulous assessment of this work. They thank Arkema for providing samples and their help to progress this work.

REFERENCES

(1) Orive, G.; Hernandez, R. M.; Gascon, A. R.; Callafiore, R.; Chang, T. M. S.; Hortelano, G. *Nature Med.* **2003**, *9*, 104–107.
(2) Goosen, M. F. A.; O'Shea, G. M.; Gharapetian, H. M.; Chou, S.; Sun, A. M. *Biotechnol. Bioeng.* **1985**, *27* (2), 146–150.
(3) Deng, Q.; Anilkumar, A. V.; Wang, T. G. *J. Fluid Mech.* **2007**, *578*, 119–138.
(4) Tomotika, S. *Proc. R. Soc. London, A* **1935**, *150*, 322–337.
(5) Southern, J. H.; Ballman, R. L. *J. Appl. Polym. Sci.* **1973**, *20*, 175.
(6) Everage, A. E. *Trans. Soc. Rheol.* **1973**, *17*, 629.
(7) Lee, B. L.; White, J. L. *Trans. Soc. Rheol.* **1974**, *18*, 467.
(8) Southern, J. H.; Ballman, R. L. *J. Polym. Sci.* **1975**, *13*, 863.
(9) Dooley, J.; Hyun, K. S.; Hughes, K. *Polym. Eng. Sci.* **1998**, *38*, 1060–1071.
(10) Wilson, G. M.; Khomami, B. *J. Non-Newtonian Fluid Mech.* **1992**, *45*, 355–384.
(11) Theofanous, G.; Nourgaliev, R.; Khomami, B. *J. Non-Newtonian Fluid Mech.* **2007**, *143*, 131–132.
(12) Yih, C. S. *J. Fluid Mech.* **1967**, *27*, 337–352.
(13) Zhao, R.; Macosko, C. W. *J. Rheol.* **2002**, *46* (1), 145–167.
(14) Schrenk, W. J.; Bradley, N. L.; Alfrey, T. J.; Maack, H. *Polym. Eng. Sci.* **1978**, *18* (08), 620.

(15) White, J. L.; Ufford, R. C.; Dharod, K. R.; Price, R. L. *J. Appl. Polym. Sci.* **1972**, *16*, 1313–1330.
(16) Khomami, B. *J. Non-Newtonian Fluid Mech.* **1990**, *37*, 19–36.
(17) Joseph, D. D. *Fluid Dynamics of Viscoelastic Liquids*; Springer : New York, 1990.
(18) Karagianis, H. A. N.; Vlachopoulos, J. *Rheol. Acta* **1990**, *29*, 71–81.
(19) Lamnawar, K.; Maazouz, A. *Polym. Eng. Sci.* **2009**, *49*, 727–739.
(20) Boonen, E.; Van Puyvelde, P.; Moldenaers, P. *J. Rheol.* **2010**, *54* (6), 1285–1306.
(21) Boonen, E.; Van Puyvelde, P.; Moldenaers, P. *ACS Appl. Mater. Interfaces* **2010**, *2* (7), 2140–2146.
(22) Jeelani, S. A. K.; Windhab, E. J. *Chem. Eng. Sci.* **2009**, *64*, 2718–2722.
(23) Sourki, A. F.; Huneault, M. A.; Bousmina, M. *Polymer* **2009**, *50*, 645–653.
(24) Hobbs, S. Y.; Dekkers, M. E. J.; Watkins, W. H. *J. Mater. Sci.* **1988**, *23*, 1225–1230.
(25) Luo, H.; Pozrikidis, C. *Comput. Fluids* **2009**, *38*, 564–571.
(26) Scribben, E.; Aaron, P. R.; Baird, G. D. *J. Rheol.* **2005**, *49*, 1159.
(27) Nemirovski, N.; Siegmann, A.; Narkis, M. *J. Macromol. Sci., Part B: Phys.* **1995**, *34*, 459–475.
(28) Gupta, A. K.; Srinivasan, K. R. *J. Appl. Polym. Sci.* **1993**, *47*, 167–184.
(29) Hemmati, M.; Nazokdast, H.; Panahi, H. S. *J. Appl. Polym. Sci.* **2001**, *82*, 1129–1137.
(30) Reignier, J.; Favis, B. D.; Heuzey, M.-C. *Polymer* **2003**, *44*, 49–59.
(31) Muller, J.-D.; Bousmina, M.; Maazouz, A. *Macromolecules* **2008**, *41*, 2096–2103.
(32) Qiu, H.; Bousmina, M. *Macromolecules* **2000**, *33*, 6588–6594.
(33) Lamnawar, K.; Maazouz, A. *Rheol. Acta* **2006**, *45*, 411–424.
(34) Lamnawar, K.; Maazouz, A. *Rheol. Acta* **2008**, *47*, 383–397.
(35) Lamnawar, K.; Baudoin, A.; Maazouz, A. *Eur. Polym. J.* **2010**, *46*, 1604–1622.
(36) Owens, D. K.; Wendt, R. C. *J. Appl. Polym. Sci.* **1969**, *13*, 1741–1747.
(37) Kwak, D. Y.; Cheung, L. K.; Park, C. B.; Neumann, A. W. *Polym. Eng. Sci.* **1998**, *38*, 757–764.
(38) Wu, S. *Polymer Interface and Adhesion*; Marcel Dekker: New York, 1982.
(39) Frenkel, J. *J. Phys.* **1945**, *9*, 385.
(40) Bellehumeur, C. T.; Kontopoulou, M.; Vlachopoulos, J. *Rheol. Acta* **1998**, *37*, 270.
(41) Johnson, K. L.; Kendall, K.; Roberts, A. D. *Proc. R. Soc. London., Ser. A* **1971**, *324*, 301–313.
(42) Mazur, S.; Plazek, D. J. *Prog. Org. Coat.* **1994**, *24*, 225–236.
(43) Lin, Y. Y.; Hui, C. Y.; Jagota, A. *J. Colloid Interface Sci.* **2001**, *273*, 267–282.
(44) Fortelný, I.; Živný, A.; Jůza, J. *J. Polym. Sci., Part B: Polym. Phys.* **1999**, *37*, 181–187.
(45) Pokluda, O.; Bellehumeur, C. T.; Vlachopoulos, J. *AIChE J.* **1997**, *43*, 3253.
(46) Chang, D.-H.; Kim, J.-K. *Macromolecules* **1989**, *22*, 1914–1921.
(47) Yang, H.-H.; Chang, D.-H.; Kim, J.-K. *Polymer* **1994**, *35* (7), 1503–1511.
(48) Becu, L.; Sautereau , H.; Maazouz, A.; et al. *Polym. Adv. Technol.* **1995**, *6*, (5), 316−325.